Synthesis and characterization of carbon xerogels and MnO_2 as electrode materials for energy storage systems

B. B. Mladenova*, T. E. Stankulov, B. A. Karamanova, S. K. Veleva, V. G. Ilcheva, A. E. Stoyanova

Institute of Electrochemistry and Energy Systems, Bulgarian Academy of Sciences, G. Bonchev Str. 10, Sofia, Bulgaria

The current investigation presents some results of the synthesis of carbon xerogels and MnO_2-based materials with predefined phase composition and surface for potential application as electrodes in supercapacitors. Organic xerogels were prepared by polycondensation of resorcinol and formaldehyde. Two different methods were used for heat treatment of the previously obtained solution: microwave heating and thermal treatment in vacuum. The obtained materials were subsequently carbonized and activated in order to increase their specific surface. MnO_2-based materials were synthesized by chemical reduction in aqueous solution. All synthesized samples were structurally and morphologically characterized. The results of the current analyses demonstrate differences in the phase composition and structure of the obtained materials, reflecting on their surface properties. This creates prerequisites for in-depth study of the influence of the synthesis method, which will reflect on the electrochemical characteristics of the studied and further tested supercapacitors.

Keywords: carbon xerogels, MnO_2, electrode materials, supercapacitors, physical and electrochemical study

INTRODUCTION

In recent years, the scientific interest in cheap and environmentally friendly materials and their application in energy storage systems has increased. Their characteristics strongly depend on the electrode materials used. For example, in electrochemical supercapacitors mainly used are carbon materials with specific parameters corresponding to a number of requirements, as high electrical conductivity, high surface area, controlled surface morphology, good corrosion resistance and thermal stability, good processability and low cost of production [1, 2]. A promising carbon material is the carbon xerogel, which possesses more than the mentioned parameters - very high active surface and electrical conductivity, significant micropore volume and well-defined mesoporosity, tunable according to the synthesis conditions, and a fast and simple production process. These properties make it an ideal electrode material in various electrochemical systems and in particular in supercapacitors [3, 4].

The synthesis of carbon xerogel can be performed using sol-gel technique by drying under ambient conditions, as well as by pyrolysis of organic gel obtained by polycondensation of resorcinol and formaldehyde [5, 6]. The meso / macroporosity of carbon gels can be designed by modifying the synthesis conditions, and the microporosity can be improved by subsequent carbonization and activation treatments [7, 8].

Carbonization and activation also lead to an increase in the surface area of the xerogels, as well as in their electrical conductivity which can be further increased by introducing conductive additives into its structure [9, 10].

Different working mechanisms of hybrid supercapacitors are possible due to the electrode materials used, which in this case are usually a carbon electrode and a composite carbon matrix electrode containing an electrochemically active component. In this case, nanostructured oxides and hydroxides, providing a high reaction area, and high porosity in order to achieve better contact with the electrolytes used are very suitable [11].

A very promising electrode material for supercapacitor systems is MnO_2. This material is characterized by a high specific theoretical capacity (~ 1370 Fg^{-1}), low cost and environmental friendliness [12]. The charge storage mechanism for MnO_2 is based on the surface adsorption of cations in the electrolyte. Due to its low electronic conductivity ($\sim 10^{-6}$ Scm^{-1}), and in order to achieve high theoretical specific capacity, MnO_2 has to be used in combination with other materials with high conductivity (e.g. carbon materials and metal nanostructures, carbon nanotubes, etc.) [13].

MnO_2 exists in different crystal modifications such as α-(hollandite), β-(pyrolusite), γ-(nsutite), δ-(birnessite), k-(akhtenskite), etc. and only some of them are suitable for a particular application [14-17]. For example, according to the research of Song

---

* To whom all correspondence should be sent:
E-mail: *borislava.mladenova@iees.bas.bg*

[14] it has been established that α-MnO$_2$ shows very good electrochemical properties as an electrode material in electrochemical current sources and especially in supercapacitors. Depending on the synthesis methods used, different structural modifications of MnO$_2$ can be obtained.

The most commonly used methods for the preparation of manganese dioxide are: microwave-assisted reflux rapid synthesis [18], hydrothermal process [19, 20], electrochemical method [21], biosynthesis [22], co-precipitation method [23, 24], sonochemical synthesis [25], etc.

The aim of the present work is to synthesize carbon xerogel and MnO$_2$ as electrode materials in energy storage systems, as well as to trace the effect of the synthesis conditions on the morphology and structure of the obtained carbons. Preliminary galvanostatic charge/ discharge tests in a two-electrode symmetric supercapacitor cell will be applied to evaluate the electrochemical characteristics of the electrode materials and their stability.

EXPERIMENTAL

Synthesis of materials

Carbon xerogels. Organic xerogels were synthesized by polycondensation of mixtures of resorcinol C$_6$H$_6$O$_2$ (99%, Valerus Co., Bulgaria) and formalin (37% aqueous solution, Valerus Co., Bulgaria) in deionized water, following the procedure described by Canal-Rodriguez *et al*. [26]. The pH of the solution is a very important factor controlling the porosity of the final carbon and therefore its precise control is very important [7]. In this case, the pH of the solution was adjusted with NaOH. Two different approaches were used for gelling, curing and gel preparing: microwave heating (treatment time about 25 minutes, RFCA_MW) and vacuum heat treatment (treatment time about 50 hours, RFCA_TT).

Manganese oxide was synthesized by precipitation from an aqueous solution of potassium permanganate (VII) KMnO$_4$ (Valerus Co., Bulgaria) and manganese (II) chloride MnCl$_2$ (Valerus Co., Bulgaria) [27]. A solution containing 0.05M MnCl$_2$ was added dropwise during 60 minutes under continuous stirring to a solution containing 0.05M KMnO$_4$. The so-obtained suspension was stirred for 6 h during which a precipitate was formed. The liquid was decanted for 24 h and a suspension of two distinct phases was formed consisting of a fine precipitate and a supernatant liquor. The precipitate was washed with deionized water. The formed precipitate was finally dried at 80 °C under vacuum and then the

manganese oxide powder was thermally treated at 200 °C.

The obtained materials were structurally characterized by X-ray diffraction (XRD) using a Philips X-ray diffractometer PW 10301030 having θ-2θ Bragg-Brentano geometry, with Cu Kα radiation (30 kV, 20 mA) at a wavelength λ = 1.5418 Å. The porous texture of the samples was examined by low-temperature (77.4 K) nitrogen adsorption using Quantachrome Autosorb iQ Station 3 instrument. The specific surface area was evaluated by the Brunauer-Emmett-Teller (BET) method at a relative pressure p/p_o in the range of 0.10-0.30. The total pore volume was calculated according to Gurwitsch's rule at p/p_o = 0.99. The pore size distribution was estimated by using the Barrett-Joyner-Halenda method.

The thermal behavior was investigated by differential thermal analysis (DTA) and thermogravimetric (TG) technique by means of a Perkin Elmer-Diamond apparatus, in air atmosphere and corundum crucibles. Powder samples with weight of 10-12 mg were heat- treated at 20 °C/min up to 1000 °C.

The samples morphology was observed by transmission electron microscopy (TEM) on a JEOL JEM 2100, 80-200 kV (Jeol Ltd. Japan) and scanning electron microscopy (SEM) using SEM Philips 515.

The obtained carbon xerogels were analysed by galvanostatic experiments. The supercapacitor cell comprised two identical electrodes containing activated carbon (80 wt.%), graphite ABG 1005 EG-1 (10 wt.%) and polytetrafluoroethylene binder (PTFE, 10 wt.%). The electrodes were assembled in a cell using Viledon 700/18 F separator and basic electrolyte 6 M KOH. The charge-discharge cycling tests were performed using an Arbin Instrument System BT-2000. The supercapacitor cells were cycled between 0.05 and 1.2 V at a current load increasing stepwise from 30 to 1200 mAg^{-1} for 25 cycles per step. Selected cells were charged/discharged up to 5000 cycles at a current rate of 240 mAg^{-1}.

The specific discharge capacitance (F g^{-1}) was calculated by the Equation [28]:

$$C = (I \times \Delta t)/(m \times \Delta V) \qquad (1)$$

where I, Δt, m and ΔV are discharge current, discharge time, mass of active material and voltage window, respectively. On the basis of the specific discharge capacitance, the energy density (E) and power density (P) can be expressed as [12]:

$$E = C \, \Delta V^2 /7.2 \qquad (2)$$
$$P = E/t \qquad (3).$$

RESULTS AND DISCUSSION

Physicochemical characterization

Carbon xerogels. The thermal decomposition of the two xerogels was analyzed by DTA / TG experiments. Figure 1 compares the thermogravimetric and DTA curves for RFCA_MW and RFCA_TT. The results show that at low temperatures, up to 300-400 °C, the carbon materials stay almost unchanged with a slight mass loss of 2-5 %, due to the presence of water. This fact is supported by the small peak of DTA between 50-80 °C. It can also be seen that the complete combustion of RFCA_RW takes place between 450 and 750 °C with only negligible residue (1%). For RFCA_TT this range is narrower, in the range of 300 and 550 °C, i.e. RFCA_TT burns relatively faster than RFCA_MW. The observed difference in the thermal decomposition of carbon xerogels obtained by different methods is probably related to the difference in their structures. For RFCA_MW, it is more complex and obviously more difficult to burn.
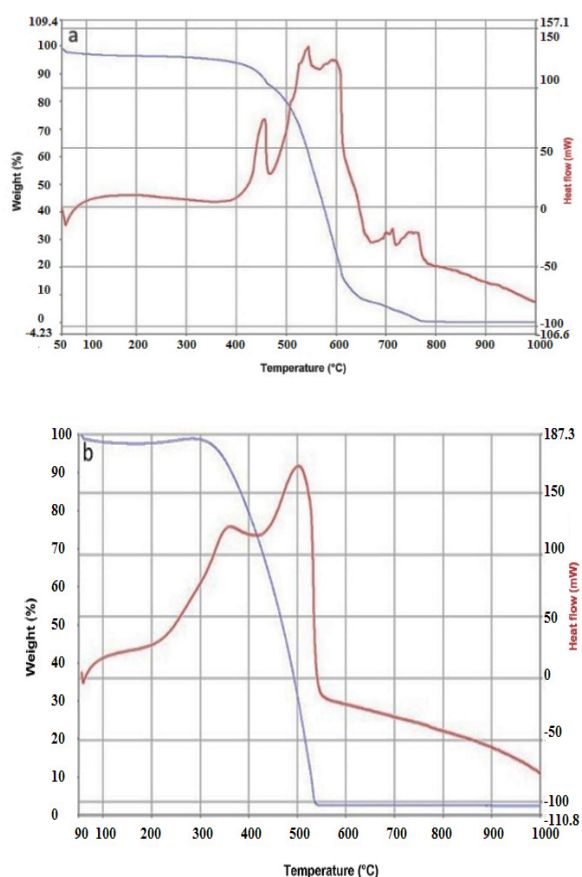

Fig. 1. Thermogravimetric and DTA curves for RFCA_MW (a) and and RFCA_TT (b)

To check the sample morphology, TEM images were taken (Fig. 2). The micrographs of both carbon xerogels show the formation of a micro layered structure with crystalline and amorphous sections. The layers are interconnected and overlap with each other.
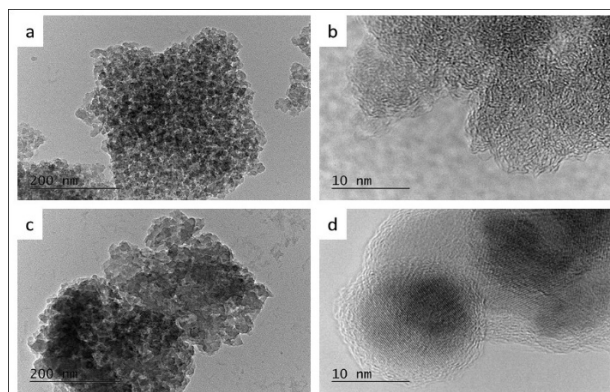

Fig. 2. TEM micrographs of carbon xerogel obtained by: microwave-induced synthesis (a, b) and vacuum heat treatment (c, d)

Figure 3 gives the pore size distribution curves for RFCA_MW and RFCA_TT together with adsorption/desorption curves. The calculated specific surface area and the total pore volume for both carbons are listed on Table 1. In general, both samples display high specific surface area, especially for RFCA_MW reaching a value higher than 660 m^2g^{-1}. The average pore diameter is very close for both RFCA_MW and RFCA_TT: 3.8 *versus* 3.7 nm (Table 1). However, the pore size distribution is different. For RFCA_TT, the distribution curve is extremely narrow with a higher peak at about 6 nm, while for RFCA_MW the distribution curve shows two peaks at 5.2 and 7.1 nm. Both isotherms are of type II and III, which is characteristic of macroporous structures [29].

Characterization of MnO₂

X-ray diffraction pattern of the synthesized MnO₂ is shown in Fig. 4. The analysis shows the presence of two broad peaks (211, 112) located at 37 ° and 66.5 °. These peaks indicate the presence of α-MnO₂ with a crystalline structure, which is confirmed by PCPDFMIN, ICDD, 2021, № 00-044-0141 database [30].
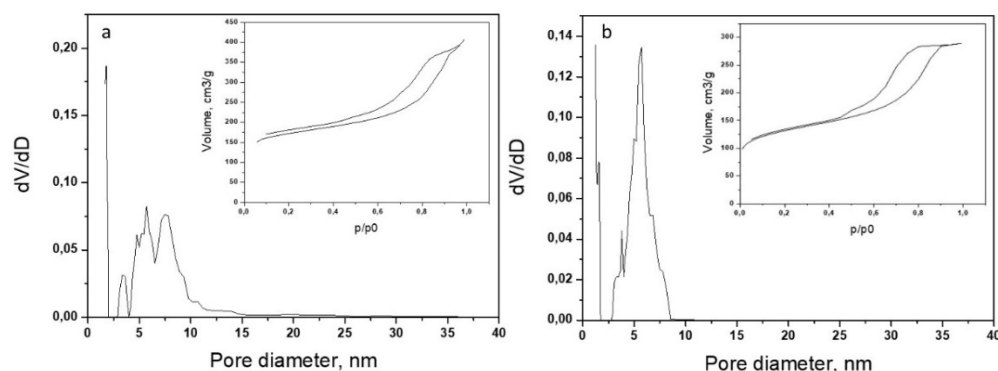
Fig. 3. Pore size distribution curves for RFCA_MW (a) and RFCA_TT (b)

Table 1. Main texture parameters of the obtained carbon xerogels: specific surface area (S_{BET}), micropore surface area (S_{micro}), external surface area (S_{ext}), total pore volume (V_t), micropore volume (V_{micro}) and average pore diameter (D_{av})

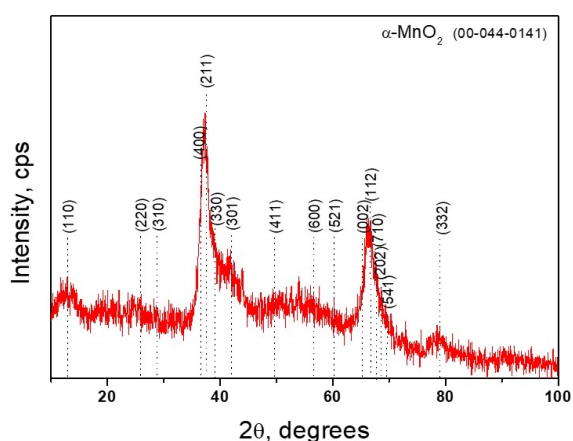| Sample	S_{BET}, m^2 g^{-1}	S_{micro}, m^2 g^{-1}	S_{ext}, m^2 g^{-1}	V_t, cm^3 g^{-1}	V_{micro} cm^3 g^{-1}	D_{av} nm
RFCA_MW	667	457	210	0.63	0.18	3.8
RFCA_TT	482	291	191	0.45	0.12	3.7
MnO$_2$	255	-	17	0.07	-	16

Fig. 4: X-ray powder diffraction pattern of MnO$_2$, compared to a database PCPDFMIN, ICDD, 2021, № 00-044-0141.

The thermal decomposition of MnO$_2$ was analyzed by DTA/TG experiments, and its thermogravimetric and DTA curves are compared in Figure 5. The results show that no intensive combustion takes place in this case.

The loss of mass up to about 200 °C can be explained by the separation of water from MnO$_2$ nanoparticles. At higher temperatures, however, a loss of about 5% of the sample mass is observed, which indicates the presence of impurities in it. The endothermic peak, observed on the DTA curve at ~ 520 ^{0}C is, could be ascribed to α-MnO$_2$ – γ-MnO$_2$ phase transition.
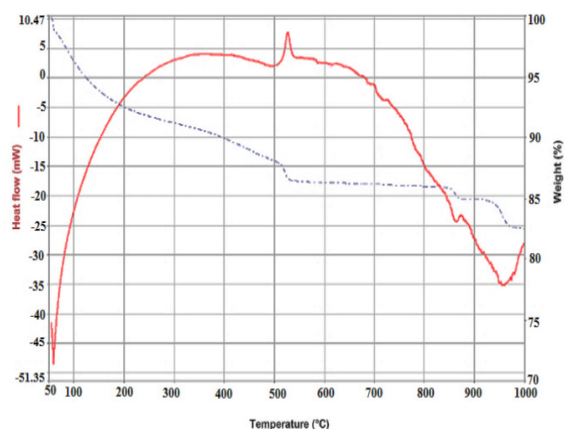

Fig. 5. Thermogravimetric and DTA curves for MnO$_2$.

The morphology of the samples was studied by SEM and TEM. Figs. 6 and 7 show the morphology of α-MnO$_2$ nanoparticles at different magnification. Fig. 6 shows that the prepared MnO$_2$ nanoparticles are homogeneous with a spherical shape and dimensions of about 50 nm. The formation of individual agglomerates with sizes over 200 nm is observed in places.

TEM images show particle aggregation, a network, which is a prerequisite for a high surface area and better electrical conductivity of the material.
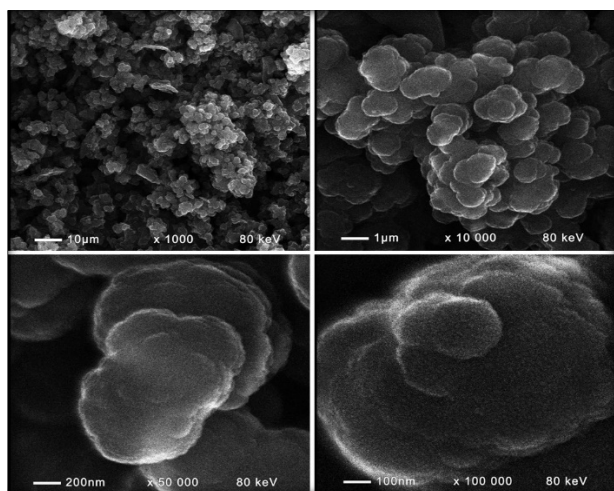
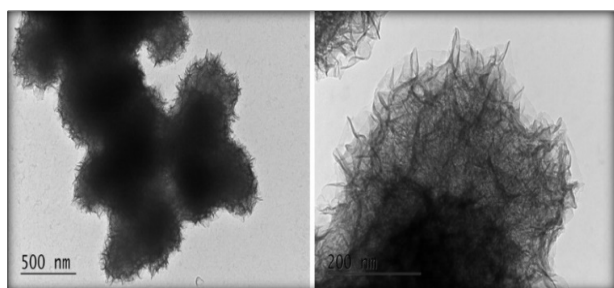**Fig. 6.** SEM image for α-MnO$_2$ nanoparticles at different magnifications.

Fig. 7. TEM image for α-MnO$_2$ nanoparticles at different magnifications.

The BET analysis and main texture parameters of the obtained α-MnO$_2$ confirm this assumption. The synthesized manganese oxide shows a high specific surface area of 255 m^{2}g^{-1} (Table 1) with isotherm type III [29] and a relatively low total pore volume. There is a narrow pore size distribution mainly in the range between 3 and 5 nm, as well as presence of macropores with sizes over 50 nm (Fig. 8).

Electrochemical results

The results of the physicochemical analysis indicate that the synthesis methods used are suitable for the preparation of electrode materials applicable in energy storage systems. It was also demonstrated that the synthesis conditions affect the structural and morphological characteristics of the obtained carbon xerogels. The RFCA_MW texture parameters show a higher surface area and volume of the micropores compared to the vacuum heat treated carbon (RFCA_TT) (Table 1).
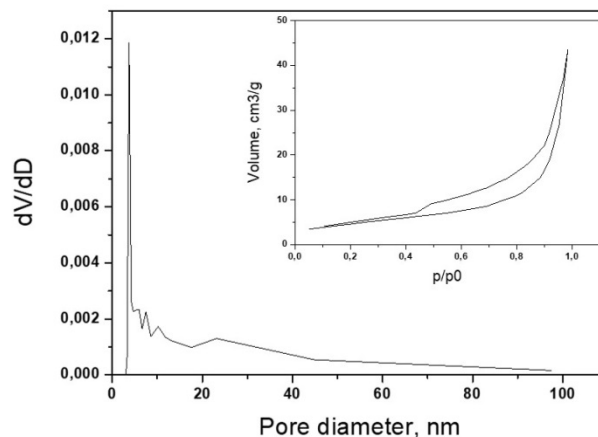

Fig. 8. Pore size distribution curves for the obtained MnO$_2$ (the inset shows the adsorption-desorption isotherms).

This result gave us reason to start electrochemical tests with carbon xerogel obtained by microwave synthesis as an electrode material in symmetrical supercapacitors. In Figure 9 its capacitive behavior as a function of current density in the current range from 60 to approximately 1200 mA g^{-1}, as well as the conducted long-term test can be seen.

The results demonstrate that the developed supercapacitor based on carbon xerogel RWCA_MW shows stable discharge capacitance of the charge-discharge process in the whole range of current loads. As one can also see, the discharge curve is clearly symmetric with its corresponding charge counterparts that exhibit a negligible voltage drop (iR-drop), indicating a rapid I-V response and an excellent electrochemical reversibility. For 5000 charge/discharge cycles, this SC displays only 5-7 % drop in discharge capacitance and over 97% efficiency (Fig. 9).
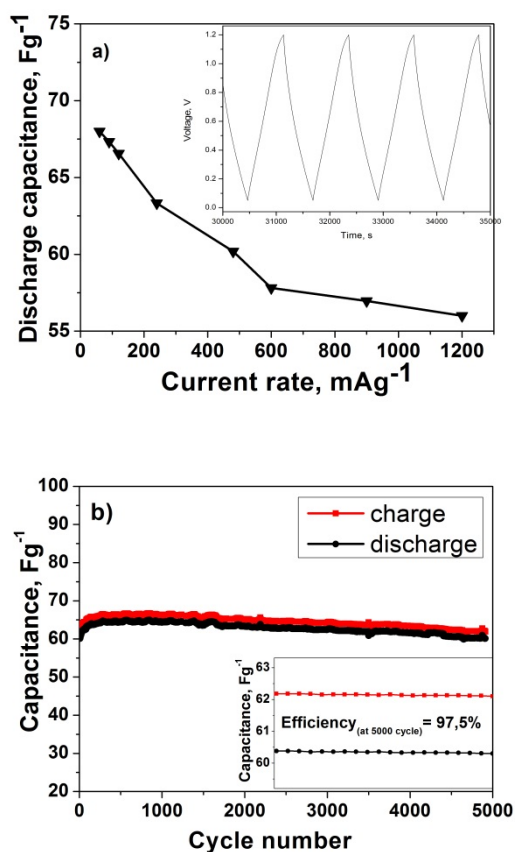
Fig. 9. Discharge capacitance as a function of current rate (a) and long-term tests at 240 mAg^{-1} (b) for symmetric supercapacitors with RWCA_MW carbon xerogel in 6 M KOH. The inset shows the galvanostatic charge-discharge curves at 240 mAg^{-1}.
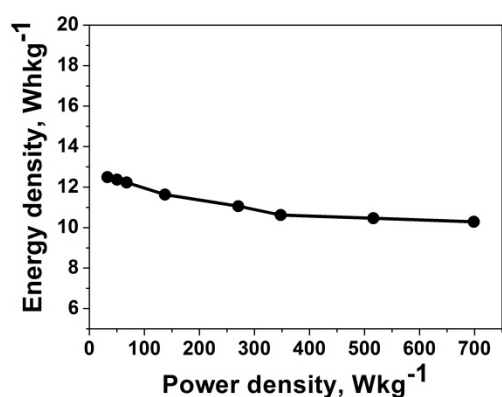

Fig. 10. Ragone plot of a symmetric supercapacitor with RWCA_MW carbon xerogel.

To evaluate the electrochemical performance of the synthesized xerogel, Figure 10 shows the Ragone plot for the assembled supercapacitor. The data indicate that the SC delivers a specific energy density of 12Wh kg^{-1} at a power density of 50 W kg^{-1}, and maintains a relatively high energy density of 10 Wh kg^{-1} even at a high power density of 700 W kg^{-1}. These values of energy density are

comparable and, in some cases, higher than those obtained for symmetric SCs in aqueous electrolyte, summarized by Zhong *et al*. [31].

CONCLUSION

Carbon xerogels and α-MnO₂ were successfully synthesized and structurally and morphologically characterized. The results of the physicochemical analysis indicate that the synthesized materials are suitable for application as electrode materials in supercapacitors. The carbon xerogels produced by microwave heating show a larger surface area and micropore volume compared to carbon materials obtained by vacuum heat treatment (RFCA_TT) and therefore this material was subjected to electrochemical test in symmetric supercapacitors.

The symmetrical supercapacitor based on RFCA_MW in 6M KOH electrolyte demonstrates a stable discharge capacitance and a high effectiveness of charge-discharge process. These results could be used as an initial research and a guide for further improvement of the carbon xerogels activation conditions in order to achieve a larger surface area and a correspondingly higher capacitance, as well as to develop a hybrid supercapacitor with the α-MnO₂ obtained.

REFERENCES

1. H. Chen, L. Hu, Y. Yan, R. Che, M. Chen, L. Wu, *Adv. Energy Mater*., **3,** 163611 (2013).
2. G. Ramos-Fernández, M. Canal-Rodríguez, A. Arenillas, J. Menéndez, I. Rodríguez-Pastor, I. Martin-Gullon, *Carbon,* **126**, 456 (2018).
3. E. G. Calvo, E. J. Juárez-Pérez, J. A. Menéndez, A. Arenillas, *J. Colloid Interface Sci*., **357**, 541 (2011).
4. E. J. Juárez-Pérez, E. G. Calvo, A. Arenillas, J. A. Menéndez, *Carbon,* **48**, 3293 (2010).
5. M. Samanc, E. Daş, A. B. Yurtcan, *Carbon Lett.,* **31**, 1287 (2021).
6. C. Alegre, M. E. Gálvez, R. Moliner, V. Baglio, A. S. Aricò, M. J. Lázaro, *Appl. Catal.,* B, **147**, 947 (2014).
7. S. A. Al-Muhtaseb, J. A. Ritter, *Adv. Mater.,* **15**, 101 (2003)
8. N. Rey-Raap, J. A. Menendez, A. Arenillas*, Carbon,* **78**, 490 (2014).
9. M. Canal-Rodríguez, J. A. Menendez, A. Arenillas, *IntechOpen*, 69 (2017).
10. M. Canal-Rodríguez, J. A. Menendez, M. A. Montes-Moran, A. Arenillas, *J. Electroanal. Chem.,* **836**, 45 (2019).
11. A. G. Pandolfoand, A. F. Hollenkamp, *J. Power Sources*, **157**, 11 (2006).

12. J. Huang, P. Xu, D. Cao, X. Zhou, S. Yang, Y. Li, *J. Power Sources,* **246**, 371 (2014).
13. Ch. Du, N. Pan, *Nanotechnology Law & Business*, 569 (2007).
14. Zh. Song, Wei Liu, M. Zhao, Y. Zhang, G. Liu, Ch. Yu, J. Qiu, *J. Alloys Compd.*, **560**, 151 (2013).
15. M. Najafpour, S. Allakhverdiev, *Int. J. Hydrogen Energy,* **37**, 8753 (2012).
16. T. Lin T, L. Yu, M. Sun, G. Cheng, B. Lan, Z. Fu, *Chem. Eng. J.*, **286**, 114 (2016).
17. V. Štengl, D. Králová, F. Opluštil, T. Němec, *Microporous and Mesoporous Mater.*, **156**, 224 (2012).
18. X. Zhang, X. Sun, H. Zhang, D. Zhang, Y. Ma, *Electrochim. Acta,* **87**, 637 (2013).
19. M. Babu Poudel, M. Shin, H. Joo Kim, *Int. J. Hydrogen Energy*, **46**, 474 (2021).
20. X. Bai, X. Tong, Y. Gao, W. Zhu, C. Fu, J. Ma, T. Tan, C. Wang, Y. Luo, H. Sun, *Electrochim. Acta,* **281***, 525 (2018).
21. M. Mahmudi, W. Widiyastuti, P. Nurlilasari, S. Affandi, H. Setyawan, *J. Ceram. Soc. Japan,* **126**, 906 (2018).
22. S. O. Ogunyemi, F. Zhang, Y. Abdallah, M. Zhan, Y. Wang, G. Sun, W. Qiu, B. Li, Artif, *Cells Nanomed. Biotechnol.*, **47,** 2230 (2019).
23. C. Kahattha, S. Santhaveesuk, *Ferroelectrics,* **552**, 121 (2019).
24. K. A. Omar, *International Journal of Research in Engineering & Technology*, **2**, 241 (2014)
25. B. S. Raj, A. M. Asiri, A. H. Qusti, J. J. Wu, *Ultrason. Sonochem.*, **21**, 1933 (2014).
26. M. Canal-Rodríguez, L. A. Ramírez-Montoya, S. F. Villanueva, S. L. Flores-López, J. A. Menéndez, A. Arenillas, M. A. Montes-Morán, *Carbon*, **152**, 704 (2019).
27. P. Staiti, F. Lufrano, *Electrochim. Acta*, **55**, 7436 (2010).
28. T. Wang, S. Zhang, X. Yan, M. Lyu, L. Wang, J. Bell, *ACS Appl. Mater. Interfaces*, **9**, 15510 (2017).
29. K. S. W. Sing, *Pure Appl. Chem.*, **57,** 603, (1985).
30. P. Wang, Y.-J. Zhao, L.-X. Wen, J. Chen, Zh.-G. Lei, *Ind. Eng. Chem. Res.*, **53**, 20116 (2014).
31. C. Zhong, G. Deng, H. Hu, J. Qiao, L. Zhang, J. Zhang, J. *Chem. Soc. Rev.*, **44**, 7484 (2015).